Splashing Onset in Dense Suspension Droplets

Ivo R. Peters, Qin Xu, and Heinrich M. Jaeger

Phys. Rev. Lett. **111**, 028301 — Published 9 July 2013

DOI: 10.1103/PhysRevLett.111.028301

Splashing onset in dense suspension droplets

Ivo R. Peters,* Qin Xu, and Heinrich M. Jaeger
James Franck Institute, The University of Chicago, Chicago, Illinois 60637, USA.
(Dated: June 7, 2013)

We investigate the impact of droplets of dense suspensions onto a solid substrate. We show that a global hydrodynamic balance is unable to predict the splash onset and propose to replace it by an energy balance at the level of the particles in the suspension. We experimentally verify that the resulting, particle-based Weber number gives a reliable, particle size and density dependent splash onset criterion. We further show that the same argument also explains why in bimodal systems smaller particles are more likely to escape than larger ones.

PACS numbers: 82.70.Kj, 47.50.-d, 47.57.Gc, 45.70.Mg

Splashing of liquid droplets upon impact on a solid surface has been investigated for over a century [1–11]. More recently, there has also been a growing interest in what happens to the spreading and splashing if particles are added to the liquid [12–14]. On micron scales, ZrO_2 suspensions have been used in studies aiming to optimize ink-jet printing applications [15–19], and on truly macroscopic scales there has been the development of 3D printers that dispense cement slurry [20, 21]. In all of these situations, an important concern is to prevent splashing, and particles from escaping, when droplets hit a surface. However, the question of when and why particles are ejected has remained unsettled, and existing experimental studies mostly focus on dilute suspensions.

Current models for suspension drop impact associate the onset of splashing with the condition that $K = We_d^{1/2} Re_d^{1/4}$ exceeds a critical value K_0, which has been the traditional criterion for pure liquid splashing on dry surfaces at atmospheric pressure in a regime independent of surface roughness [4, 22, 23]. Here the Weber and Reynolds numbers are defined as $We_d = \rho_l r_d U^2/\sigma$ and $Re_d = \rho_l r_d U/\mu$, with r_d the droplet radius, U the droplet impact velocity, and ρ_l, σ and μ the liquid density, surface tension and dynamic viscosity, respectively.

In these models, the addition of particles has been captured by replacing μ with an effective viscosity μ_e that increases with packing fraction [12, 24–28]. This predicts that a droplet of a pure liquid that would splash under certain conditions should not splash after adding enough particles. To our knowledge, there exists no systematic study that confirms this prediction. In fact, Nicolas observed [12] that adding particles, instead, lowered the splashing threshold K_0.

To investigate the influence of added particles, we depart from the dilute limit described above, and instead focus here on the limit of dense granular suspensions with volume packing fractions $\phi = 0.62 \pm 0.03$, where the discrepancy with the above droplet-scale splash onset criterion is most pronounced.

In pure liquid droplets, the size of the ejecta depends on either the destabilization of a thin liquid sheet [5, 29–34] or, in the case of prompt splashing, on an instability at the moving contact line [5, 10, 35]. At splash onset in a suspension, on the other hand, the ejecta are the solid particles (see Fig. 1), which implies a built-in length scale. This length scale was not taken into account in the energy balance leading to K, and not considered by Refs. [12, 18, 19]. We will now evaluate the energy balance at the particle level, which we will then compare to our experiments.

Energy balance.–Surface tension keeps particles inside the drop because an escaping particle involves an increase of the surface energy, which scales with the particle surface area [37]

$$E_{surf} \sim 4\pi r_p^2 \sigma, \tag{1}$$

where r_p is the particle radius. A particle can thus escape if it has enough kinetic energy, $E_{kin} = \frac{2}{3}\pi\rho_p r_p^3 u_p^2$, with ρ_p the specific density of a particle and u_p its velocity, to overcome surface tension. The velocity u_p is a result of collisions between neighboring particles (see Fig. 2), which convert vertical into horizontal velocities. Based on momentum conservation we expect that the velocity u_p of a particle sitting on the outer surface of a droplet will be similar to the impact velocity of the drop U. The ratio of the kinetic and surface energy then is

$$\frac{E_{kin}}{E_{surf}} \sim \frac{1}{6}\frac{\rho_p r_p U^2}{\sigma} \equiv \frac{1}{6} We_p. \tag{2}$$

Here, We_p is a particle-based Weber number. Fig. 1(*p*-*s*) shows an example below and above the splashing onset.

Experiments.–We prepared suspensions of demineralized water with ZrO_2 (Glenn Mills) and soda-lime glass (Mo-Sci) particles inside a syringe. Particles were spherical, with standard deviations from their mean size of 5 to 8% for the ZrO_2 and 15 to 20% for the glass beads and densities $\rho_p = (3.9 \pm 0.1) \cdot 10^3$ kg/m^3 and $\rho_p = (2.53 \pm 0.02) \cdot 10^3$ kg/m^3, respectively. The volume fractions were determined by measuring the mass of a suspension drop, letting the water evaporate on a hot plate, and then measuring the mass of the dry particles. All packing fractions were between 59 and 65%. They are probably slightly overestimated due to finite sample size,

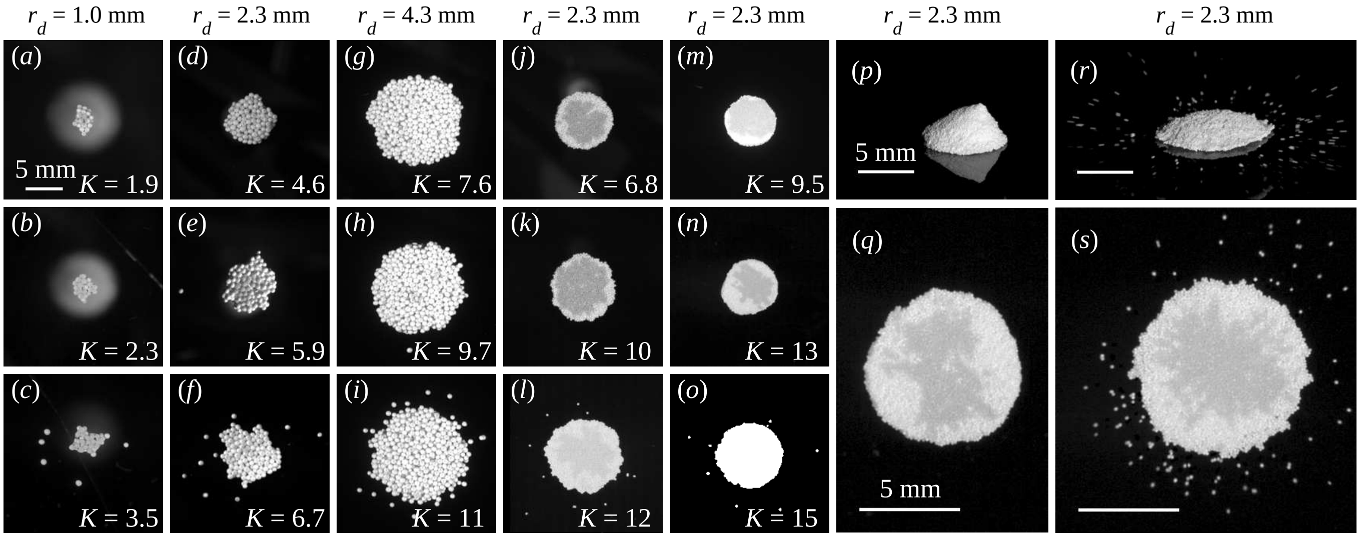

FIG. 1. Still images right after impact of ZrO_2 particles in water onto a smooth glass plate, for different droplet radii r_d (see text above the images) and particle radii: (*a-i*) $r_p = 362$ μm, (*j-l*) $r_p = 138$ μm, (*m-s*) $r_p = 78$ μm. The time between impact and ejection of the first particles ranges from 0.6 to 3.5 ms. Images (*a-o*) are organized in vertical columns, with drop impact speed and therefore K increasing from top to bottom to bracket the onset of splashing, defined as the ejection of individual particles. For the K values listed in the top/middle/bottom rows we never/sometimes/always observed particle ejection. $K = We_d^{1/2} Re_d^{1/4}$, where we used the effective viscosity μ_e given by Krieger and Dougherty [26] in Re_d. The blurred background in (*a*) and (*b*) is the out-of-focus image of the syringe. Note that (*o*) has been thresholded and dilated in order visualize the ejected particles that would otherwise be invisible due to their small size. (*p*,*q*) side and bottom view of a droplet that does not splash ($We_p = 12$), (*r*,*s*) side and bottom view of a splashing droplet ($We_p = 26$). The scale bar in the images is 5 mm, images (*a-o*) all have the same scale. See also Ref. [36].

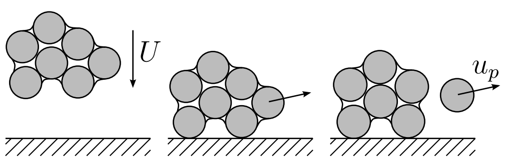

FIG. 2. Sketch of the ejection mechanism upon impact.

because the amount of liquid depends on the shape of the menisci between the particles sitting at the surface of the droplet. In the current study we focus on changes to inviscid liquid splashing introduced by the particles and do not explore the role of additional viscous dissipation from the suspending liquid [38].

Drops were formed by slowly pushing the suspension out of a cylindrical nozzle using a syringe pump. As gravity pulls the suspension down, a pinch-off will occur [39, 40], resulting in highly reproducible suspension drops. We varied U by adjusting the release height, and r_d by changing the nozzle size. During extrusion of the suspension there is only minimal deformation of the droplet, producing a droplet radius equal to the nozzle radius [41]. The experiments were recorded with a Phantom V12 high speed camera at frame rates of $6.2-10$ kHz with a 105 mm Micro-Nikkor lens, resulting in a resolution of $20-50$ μm/pixel. We used bottom views to observe and track particles ejected after impact. Typical bottom views are shown in Fig. 1(*a-o*). We never observed the ejection of liquid droplets in our experiments.

To determine the transition velocity U^* above which particles are ejected from the droplet, we determine the lower (upper) bound of U^* (represented by the error bars in Fig. 3) at which we never (always) see ejected particles. Because we are able to distinguish individual particles, we define a non-splashing experiment when not a single particle leaves the suspension. A particle has left the suspension when there is no liquid bridge connecting it to the other particles. The experimental determination of U^* for the cases of $r_p = 78$ μm and $r_p = 362$ μm ZrO_2 particles is shown in Fig. 4(*a*), where N_S is number of times we observe a splash and N is the number of times we repeat one impact speed U (typically 10 times).

Unimodal suspensions–Fig. 1 verifies that a global criterion, $K > K_0$, does not capture the observed behavior. Within these examples there is about a factor 5 difference in K_0-values for droplets comprised of the same liquid and similar packing fraction of ZrO_2 beads. Note that in Fig. 1(*a-i*) the particles all have the same size. Fig. 3 shows the influence of particle size on the splash transition. In all cases, the transition to splashing happens at the same value $We_p \approx 14$. This is consistent with Eq. (2), where We_p is the relevant parameter for the splash onset [42]. Possible non-Newtonian effects or an effective viscosity seem to play no role here. Com-

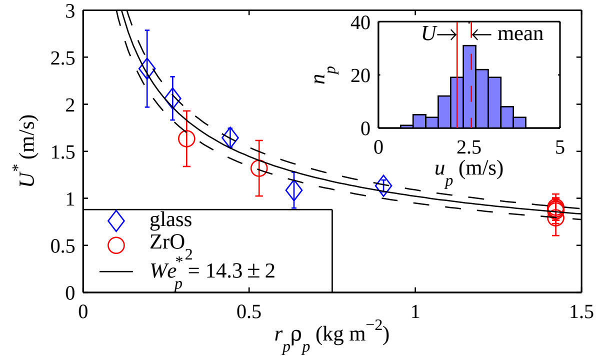

FIG. 3. Splash onset velocity U^* as function of the product of particle radius r_p and particle density ρ_p. The cluster of 7 data points at the far right corresponds to 3 different drop sizes (see also Figs. 1, 4) and substrates with 4 different roughnesses (see main text), all other data are for $r_d = 2.3$ mm on a smooth substrate. The solid curve gives the onset Weber number ${We_p}^*$ calculated from a best fit to all experimental data. The dashed lines represent the upper and lower bounds for ${We_p}^*$, corresponding to one standard deviation. Inset: Histogram of the velocity u_p of ejected particles at $We_p = 20$, for $r_p = 78$ μm.

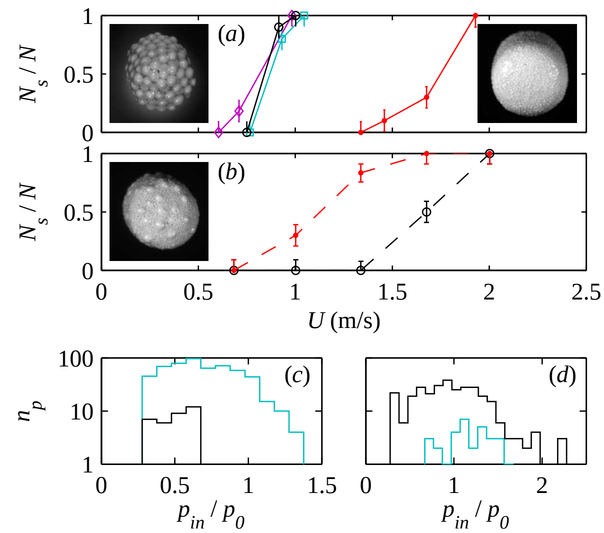

FIG. 4. Comparison between unimodal and bimodal ZrO_2 suspensions. All are data for droplets made with nozzle radius $r_d = 2.3$ mm, except for data shown in magenta and cyan in (a) for which $r_d = 1.0$ mm and $r_d = 4.3$ mm, respectively. (a) Splash onset for unimodal suspensions of large ($r_p = 362$ μm, black, cyan, and magenta open symbols) and small ($r_p = 78$ μm, red dots) particles. (b) Splash onset for bimodal suspensions with volume ratio $\sim 1 : 1$ of small to large particles. Two distinct onsets exist: one where only small particles escape, and one where both small and large particles escape. Data symbols and colors are as in (a). All insets: Examples of the unimodal and bimodal suspension droplets corresponding to the data presented in this figure, imaged from below just before impact. (c) Histogram of relative momentum changes for large particles in unimodal (cyan) and bimodal (black) suspensions at $U = 2$ m/s. (d) Same as (c), but for small particles.

paring the black, cyan, and magenta lines in Fig. 4(a) –corresponding to the cluster of data points at the far right of Fig. 3– we see that a factor of over four in r_d has no significant influence on U^* – in strong contrast with using r_d as the relevant length scale.

The inset in Fig. 3 shows a typical velocity distribution for 78 μm particles at $We_p = 20$, where the mean velocity $\bar{u}_p$ of the particles after they are ejected from the suspension is slightly higher than the impact velocity U. For the larger ZrO_2 particles tested, $\bar{u}_p$ was smaller than U and the ratio $\bar{u}_p/U$ decreases with particle size, but all measured mean velocities are in the range $0.5 < \bar{u}_p/U < 1.2$. Thus, u_p of an ejected particle is always similar to the impact speed, confirming our estimate used in Eq. (2).

Results on bimodal suspensions–From Fig. 4(a) it is clear that a suspension with particles of radius 362 μm always splashes at $U \gtrsim 1.0$ m/s. On the other hand, a suspension with particles of radius 78 μm never splashes at $U \lesssim 1.3$ m/s. So what happens if we make a bimodal suspension of these two particles types and impact at a speed between these two limits? We find that the splashing behavior is inverted: The larger particles remain inside, while the smaller particles get ejected. In Fig. 4(b) we determine the splashing behavior for the bimodal suspension the same way as we did for unimodal suspensions in Fig. 4(a). Clearly, the transition curves switch their position when going from unimodal to bimodal.

At first sight this result seems counterintuitive: surface tension should be more effective in keeping small particles inside the droplet than large particles. To qualitatively explain this we take a closer look at how the particles obtain their velocity upon impact. We have argued before that collisions between particles of the same size will result in similar velocities – which explains why u_p scales with U. Collisions between large and small particles can, however, result in much larger velocities for the small particles, which explains why the transition is at a lower impact speed. Conversely, small particles can only give little velocity to large particles. The presence of small particles also reduces the chance for direct collisions between large particles, which explains the increased transition impact speed for large particles in bimodal suspensions.

In order to extract the change in momentum due to the impact, we perform experiments for all three suspension configurations at an impact speed of 2 m/s where we always find ejected particles: (i) unimodal suspensions with $r_p = 362$ μm, (ii) unimodal suspensions with $r_p = 78$ μm, and (iii) bimodal suspensions consisting of the same two different particles sizes. We calculate the gain in momentum due to the collisions as follows: We first determine the velocities of the ejected particles and calculate their kinetic energy. We know that during the ejection process the particle has transferred part of its kinetic energy to the surface energy given by Eq. (1). Adding this surface energy to the measured kinetic energy gives us the kinetic energy E_{in} of the particle just *before* it was ejected, which corresponds to the momentum $p_{in} = (\frac{8}{3}\pi\rho_p r_p^3 E_{in})^{1/2}$. Comparing this to the vertical momentum of the particle before the moment of impact, $p_0 = \frac{4}{3}\pi\rho_p r_p^3 U$, gives us the relative change in momentum p_{in}/p_0 due to collisions between particles.

In Fig. 4(c-d) we show p_{in}/p_0 for the three experiments mentioned above. Every impact speed was repeated 10 times and we count the number of ejected particles n_p that are within a specific range of momenta. Fig. 4(c) shows that for large particles going from unimodal suspensions (cyan) to bimodal suspensions (black), the probability of finding particles with a momentum in the order of p_0 decreases by at least an order of magnitude. Note that for the bimodal suspensions $p_{in}/p_0 \lesssim 0.75$. For small particles on the other hand (Fig. 4(d)), the probability of finding small particles with a momentum ratio > 1 is increased by more than a factor 5 when changing from a unimodal to a bimodal suspension.

Since collisions between particles are responsible for driving the onset of splashing, and less so the interaction of particles with the substrate, we expect that surface roughness will play a much smaller role than for pure liquids. To check this we performed experiments on substrates with roughness length scale ℓ ranging from $\ell > r_p$ to $\ell \ll r_p$. The results are included in Fig. 3, where in all cases there is no difference compared to the impact on a smooth surface. The same independence of the splashing onset holds for experiments performed at a reduced ambient pressure $P \approx 10$ kPa.

Conclusions and outlook.–These experiments demonstrate that the relevant parameter to quantify the splash onset is a Weber number calculated at the particle level. This is in contrast to earlier proposals for splash onset criteria in suspensions. Local interactions between particles at the edge of the droplet are responsible for the ejection of particles upon impact. This explains why the effective viscosity, which acts on a global droplet level, does not prevent the suspension from splashing. Our observations give rise to the question at which packing fraction the global droplet description breaks down and when the dense limit, investigated here, takes over. The same local interactions also drive the inversion of the splash onset for bimodal suspensions. Since the momentum transfer in dense suspensions is collision dominated, it might be possible to further tune the splash onset via particle characteristics such as shape, restitution coefficient, or friction. However, our findings already demonstrate that splash onset in dense suspensions behaves qualitatively different from predictions based on pure liquids. The typically used K parameter does not delineate the splash onset properly. Instead, a particle-based, critical Weber number ${We_p}^*$ describes the onset well.

We thank C. Stevens for reading the manuscript and her experimental setup for testing the pressure dependence, and T. Witten, and W. Zhang for insightful discussions. This work was supported by NSF through its MRSEC program (DMR-0820054) and by the US Army Research Office through grant number W911NF-12-1-0182.

* irpeters@uchicago.edu

[1] A. M. Worthington, Proc. R. Soc. A **25**, 261 (1876).
[2] M. Rein, Fluid Dyn. Res. **12**, 61 (1993).
[3] L. Xu, W. W. Zhang, and S. R. Nagel, Phys. Rev. Lett. **94**, 184505 (2005).
[4] A. L. Yarin, Ann. Rev. Fluid. Mech. **38**, 159 (2006).
[5] L. Xu, Phys. Rev. E **75**, 056316 (2007).
[6] S. Mandre, M. Mani, and M. P. Brenner, Phys. Rev. Lett. **102**, 134502 (2009).
[7] P. Tsai, M. H. W. Hendrix, R. R. M. Dijkstra, L. Shui, and D. Lohse, Soft Matter **7**, 11325 (2011).
[8] M. M. Driscoll and S. R. Nagel, Phys. Rev. Lett. **107**, 154502 (2011).
[9] L. Duchemin and C. Josserand, Phys. Fluids **23**, 091701 (2011).
[10] A. Latka, A. Strandburg-Peshkin, M. M. Driscoll, C. S. Stevens, and S. R. Nagel, Phys. Rev. Lett. **109**, 054501 (2012).
[11] S. T. Thoroddsen, K. Takehara, and T. G. Etoh, J. Fluid Mech. **706**, 560 (2012).
[12] M. Nicolas, J. Fluid Mech. **545**, 271 (2005).
[13] L.-H. Luu and Y. Forterre, J. Fluid Mech. **632**, 301 (2009).
[14] M. Guémas, A. G. Marín, and D. Lohse, Soft Matter **8**, 10725 (2012).
[15] P. F. Blazdell, J. R. G. Evans, M. J. Edirisinghe, P. Shaw, and M. J. Binstead, J. Mat. Sci. Lett. **14**, 1562 (1995).
[16] W. D. Teng, M. J. Edirisinghe, and J. R. G. Evans, J. Am. Ceram. Soc. **80**, 486 (1997).
[17] M. Mott, J.-H. Song, and J. R. G. Evans, J. Am. Ceram. Soc. **82**, 1653 (1999).
[18] K. A. M. Seerden, N. Reis, J. R. G. Evans, P. S. Grant, J. W. Halloran, and B. Derby, J. Am. Ceram. Soc. **84**, 2514 (2001).
[19] J. A. Lewis, J. E. Smay, J. Stuecker, and J. Cesarano, J. Am. Ceram. Soc. **89**, 3599 (2006).
[20] J. Pegna, Automation in Construction **5**, 427 (1997).
[21] R. Buswell, R. Soar, A. Gibb, and A. Thorpe, Automation in Construction **16**, 224 (2007).
[22] C. Mundo, M. Sommerfeld, and C. Tropea, Int. J. Multiphase Flow **21**, 151 (1995).
[23] G. E. Cossali, a. Coghe, and M. Marengo, Experiments in Fluids **22**, 463 (1997).
[24] H. Eilers, Coll. Pol. Sci. **97**, 313 (1941).
[25] M. Mooney, J. Colloid Sci. **6**, 162 (1951).
[26] I. M. Krieger and T. J. Dougherty, Trans. Soc. Rheol. **3**, 137 (1959).
[27] J. J. Stickel and R. L. Powell, Ann. Rev. Fluid. Mech. **37**, 129 (2005).
[28] C. Bonnoit, T. Bertrand, E. Clement, and A. Lindner, Phys. Fluids **24**, 043304 (2012).
[29] R. F. Allen, J. Coll. Int. Sci. **51**, 350 (1975).
[30] S. T. Thoroddsen and J. Sakakibara, Phys. Fluids **10**, 1359 (1998).
[31] S. T. Thoroddsen, J. Fluid Mech. **451**, 373 (2002).
[32] M. M. Driscoll, C. S. Stevens, and S. R. Nagel, Phys. Rev. E **82**, 036302 (2010).
[33] J. D. Ruiter, R. E. Pepper, and H. A. Stone, Phys. Fluids **22**, 022104 (2010).
[34] I. R. Peters, D. van der Meer, and J. M. Gordillo, J. Fluid Mech. **724**, 553 (2013).
[35] R. Rioboo, M. Marengo, and C. Tropea, Exp. Fluids **33**, 112 (2002).
[36] See supplementary material at [URL will be inserted by publisher] for movies of monodisperse and bidisperse suspension splashes.
[37] We neglect dewetting in this argument; typical dewetting speeds are of the order of 0.1 m/s [43, 44]. Partial dewetting would influence the actual surface energy, but keeps the scaling intact.
[38] Viscosity can play a role in either dissipating energy of escaping particles or changing the coefficient of restitution e, which is a function of the Stokes number $St = (2/9)\rho_p r_p U/\mu$ [45]. Stokes numbers for our experiments are in the range $St \approx 100..2000$, which corresponds to $e \approx 0.7..0.9$. We changed the viscosity by a factor two without observing a significant change in the splash onset. The splash onset is influenced if we change the viscosity more dramatically, i.e., by one order of magnitude, but this is outside the scope of our current study.
[39] M. Z. Miskin and H. M. Jaeger, Proc. Nat. Ac. Sc. **109**, 4389 (2012).
[40] T. Bertrand, C. Bonnoit, E. Clément, and A. Lindner, Granular Matter **14**, 169 (2012).
[41] The droplets have smooth cylindrical shapes with an aspect ratio (height:width) of approximately 1:1. The orientation of this cylinder upon impact has no noticeable influence on the ejection of suspended particles.
[42] One might expect that the transition would occur at $We_p \approx 6$, where $E_{kin} = E_{surf}$, but we stress that u_p only scales with U, and is not necessarily identical to it. Additionally, an *excess* of kinetic energy is needed in order to overcome the surface tension.
[43] T. D. Blake and K. J. Ruschak, Nature **282**, 489 (1979).
[44] K. G. Winkels, I. R. Peters, F. Evangelista, M. Riepen, A. Daerr, L. Limat, and J. H. Snoeijer, Eur. Phys. J. Special Topics **192**, 195 (2011).
[45] P. Gondret, M. Lance, and L. Petit, Phys. Fluids **14**, 643 (2002).